Check for updates

MOF nanoparticles as heterogeneous catalysts for direct amide bond formations†

Isabel Abánades Lázaro, [iD] *[a] Ross S. Forgan [iD] [b] and Francisco. G. Cirujano [iD] *[a]

The influence of composition and textural characteristics of a family of ultra-small isoreticular UiO-type metal–organic frameworks (MOFs) with different functionalized and extended linkers on their catalytic performance is evaluated. Two direct amide bond formations across four different substrates (benzylamine + phenylacetic acid and aniline + formic acid) are employed as proof-of-concept reactions to test the activity of the Zr-MOF nanoparticles. The reaction rates of amide bond formation are evaluated against physico-chemical properties such as crystallinity, porosity, particle size or linker functionality, alongside the Lewis acid and hydrophobic properties of the MOFs, in order to gain insights into the catalytic mechanism and optimal properties for its enhancement.

Introduction

The *N*-formylation of amines is an important reaction to produce amide bonds, which are ubiquitous in industrially and naturally relevant organic molecules, from pharmaceuticals to proteins.[1–5] Different strategies are employed for the synthesis of amide bonds, the reaction between carboxylic acids and amines being the most direct pathway, without requiring pre-functionalization or activation steps. The thermal reaction of amidation of carboxylic groups requires temperatures higher than 180 °C, which results in by-products due to the induction of other non-desired side reactions. Acid catalysts with an adequate density and strength of their active sites are normally successful systems to promote the activation of the carbonyl group of the acid and nucleophilic amine attack over the protonation or decarboxylation of these functionalities.[6] However, high temperatures, long reaction times and the use of solvents are still needed for successful catalysis of direct amidation.

Thus, the design of a catalyst able to favour the processes at lower temperatures, under solvent-free conditions, and to direct it towards the formation of the N–C bond between the amine and carboxylic acid, is needed. Different homogeneous and heterogeneous catalysts are reported for such endeavours, such as Brønsted (sulfonic acids, HPW, Si-OH, *etc*.) or Lewis

(Ti, Zr, Nb, Al, Zn, *etc*.) acids. In this sense, heterogeneous catalysts are preferred over homogeneous ones since their recovery and recycling is facilitated. Particularly, porous solids are a fundamental class of heterogeneous catalysts, given their high surface areas and pore volumes, ability to facilitate the dispersion of active sites, and the enhanced diffusion of substrates and products. This is indicated by pioneering interest in the application of clays,[7,8] zeolites[9] or mesoporous silica[10] to promote direct amidation reactions during the last decades.

Recently, metal–organic frameworks (MOFs) have appeared as a novel class of hybrid metal–organic porous material with a crystalline and highly tailorable structure, and they are being increasingly applied as heterogeneous catalysts.[11–16] In this sense, MOFs offer the possibility of immobilizing acid sites in the nodes of porous frameworks that allows well-defined and accessible active sites in the solid matrix.[17–21] Among all the metals employed in the synthesis of robust and active MOF-based catalysts, Zr(IV) MOFs such as the UiO family or MOF-808, which contain $Zr_6O_4(OH)_4(RCO_2)_{12}$ clusters, have been widely applied for the activation of carbonyls or other oxo-functions due to the presence of highly oxophilic coordinatively unsaturated sites (CUS).[22–25] These MOFs are also the preferred systems in acid-catalyzed direct amidation reactions between carboxylic acids and amines.[26–28] On the one hand, Timofeeva *et al.* considered either the sulphated cluster or the pore size – in the case of sulfonated MOF-808 or UiO-66, respectively[27] – as key factors for the formylation of aniline under solvent-free/MeOH room temperature conditions (see Scheme 1a).

MOF-808 outperformed pristine UiO-66 when using methanol as solvent (78% *vs.* <1% yield, respectively, at 35 °C for 90 min), although no further information on the performance of UiO-66 under solvent-free conditions was provided. On the

[a]Instituto de Ciencia Molecular (ICMol), Universitat de Valencia, Catedrático José Beltrán Martínez n° 2, 46980 Paterna, Valencia, Spain.
E-mail: isabel.abanades@uv.es, francisco.c.garcia@uv.es
[b]WestCHEM School of Chemistry, University of Glasgow, Joseph Black Building, University Avenue, Glasgow G12 8QQ, UK
†Electronic supplementary information (ESI) available. See DOI: https://doi.org/10.1039/d2dt00369d
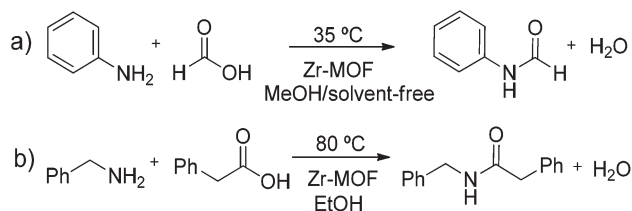
Scheme 1 (a) Formylation of aniline, and (b) reaction between phenylamine and phenylacetic acid catalysed by the CUSs of the Zr-MOFs MOF-808 and UiO-66.[27,28]

other hand, UiO-66 was also recently employed as a heterogeneous catalyst by de Azambuja, Parac-Vogt and co-workers for the reaction between benzylamine and phenylacetic acid (see Scheme 1b).[28]

Zr-dicarboxylate MOFs of the UiO-66 isoreticular series (see Fig. 1) are commonly investigated in catalysis due to the fact that the $Zr_6O_4(OH)_4$ secondary building unit (SBU) can be maintained while linkers with slight microscopic variations in the composition, such as the presence of substitutions on the aromatic ring, can be incorporated, resulting in significant changes in the macroscopic properties of the final MOF, such as the hydrophobicity, pore size or catalytic activity.[22] Indeed, employing different linkers allows fine-tuning the electronic and steric properties of the metal-oxo clusters in this highly robust Zr-UiO MOF platform.[22,23]

However, in the context of direct amide bond formation, the use of Zr-dicarboxylate MOFs and derivatives (i) under solvent-free mild conditions, (ii) with different linker functionality and size and (iii) in the form of ultra-small nanoparticles have been less explored (especially the last point) in the assessment of catalytic performance. Thus, the differences in amidation activity of isoreticular MOFs containing similar Zr-oxo clusters with different types of linkers need to be better understood.

Herein we report the synthesis, characterization and catalytic activity of ultra-small Zr-dicarboxylate MOF nanoparticles made with linkers of varied functionality and size (BDC, BDC-NH$_2$, BDC-NO$_2$, BDC-OH, NDC and BPDC), as represented in Fig. 1, in order to tune their physicochemical properties (*i.e.* porosity, organic group composition) and thus chemical reactivity towards carboxylic acid (*i.e.* phenylacetic acid and formic acid) and amine (*i.e.* aniline and benzylamine) functions. In this work, we aim to apply Zr-MOF ultra-small nanoparticles designed with different functionalities as catalysts for direct amide bond formation and to study the effect of the linker functionality and size on their catalytic activity.

Experimental

Materials

Aniline, formic acid, benzylamine, phenylacetic acid and DMSO-d_6 were purchased from Aldrich.

MOF synthesis

In separate vials, zirconyl chloride octahydrate (213 mg, 0.66 mmol) and the linker (1.65 mmol) were dissolved in 20 mL of DMF. After mixing both precursor solutions in a 80 mL jar, acetic acid (12 mmol) was added to the reaction mixture which, after gently stirring, was placed in the oven at 120 °C for 24 h. After cooling to room temperature, the powders were collected by centrifugation, and washed with DMF (X2) and MeOH (X3) through dispersion centrifugation cycles. The resultant materials were dried under vacuum for at least 24 hours prior to analysis.

Catalytic tests

For reaction A, 100 μL of aniline (1.1 mmol) and 200 μL of formic acid (5.3 mmol) were added to a glass vial containing 10 mg of MOF and the mixture was heated at 35 °C under stirring at 300 rpm. Sample aliquots were taken after 5 and 30 min of reaction, diluted with DMSO-d_6 and analyzed by ^{1}H-NMR spectroscopy. The larger peak areas corresponding to three protons of the aromatic rings of the aniline reagent and formamidine products were employed for the calculation of the yield, in order to minimize the error. For the recycling test, the spent MOF was thoroughly washed with ethanol and acetone and recovered by centrifugation. The dry MOF sample was tested in a subsequent reaction cycle.

For reaction B, 20 mg of phenylacetic acid (0.15 mmol) and 20 μL of benzylamine (0.19 mmol) were dissolved in 200 μL of methanol-d_4 and added to a vial containing 10 mg of MOF. The mixture was heated at 60 °C for 24 h under stirring at 300 rpm. Sample aliquots were taken after this time and analysed as described for the formylation reaction.

Fig. 1 Structures of Zr-dicarboxylate MOFs of the UiO topology with different linkers (Zr-BDC-X, Zr-BPDC, Zr-NDC). BDC: benzene-1,4-dicarboxylic acid. BPDC: biphenyl-4,4'-dicarboxylic acid. NDC: naphthalene-2,6- dicarboxylic acid.

Characterization

Powder X-Ray Diffraction (PXRD) patterns were collected on a PANalytical X'Pert PRO diffractometer using copper radiation (Cu Kα = 1.5418 Å) with an X'Celerator detector, operating at 40 mA and 45 kV. Profiles were collected in the 3° < 2θ < 40° range with a step size of 0.017°. (University of Valencia). Thermogravimetric Analysis (TGA) was carried out with a Mettler Toledo TGA/SDTA 851 apparatus between 25 and 800 °C under ambient conditions (10 °C min⁻¹ scan rate and an airflow of 9 mL min⁻¹). (University of Valencia). Nuclear Magnetic Resonance (NMR) Spectroscopy were recorded on either a Bruker AVIII 300 MHz spectrometer and referenced to residual solvent peaks. (University of Valencia). N_2 adsorption isotherms were carried out at 77 K on a Quantachrome Autosorb iQ gas sorption analyser. Samples were degassed under vacuum at 120 °C for 20 hours using the internal turbo pump. BET surface areas were calculated from the isotherms using the Micropore BET Assistant in the Quantachrome ASiQwin operating software. (University of Glasgow). Scanning Electron Microscopy (SEM) and single point energy-dispersive X-Ray analysis (EDX) were employed to study particle morphologies, dimensions, and mapping with a Hitachi S-4800 scanning electron microscope at an accelerating voltage of 20 kV, over samples metalized with a mixture of gold and palladium for 90 seconds. (University of Valencia). Fourier Transform Infrared Spectroscopy of solids was collected using a Shimadzu Fourier Transform Infrared Spectrometer, FTIR-8400S, fitted with a Diamond ATR unit. (University of Valencia). For the quantification of the reaction yield, we have focused on the following ^{1}H-NMR spectroscopic signals of reagents and products (see Fig. S37 and S52†). Aniline ^{1}H NMR (300 MHz, DMSO) δ 7.08 − 6.93 (m, 2H, Ar$_{ortho}$-H), 6.61 − 6.45 (m, 3H, Ar$_{meta,para}$-H). Formanilidine (*N*-Phenyl formamide). ^{1}H NMR (300 MHz, DMSO-d_6) 8.33–8.22 (brs, 1H, OC-H), 7.58 (m, 2H, Ar$_{ortho}$-H), 7.39 − 7.25 (m, 3H, Ar$_{meta,para}$-H). Phenylacetic acid (pure) δ 7.30 (m, 5H, Ar-H), 3.61 (s, 2H, CH$_2$). Benzylamine (pure) δ 7.29 (m, 5H), 3.79 (s, 2H, CH$_2$). –CH$_2$– in the reaction media: phenylacetic acid (δ 3.48); benzylamine (δ 3.97); *N*-benzyl-2-phenylacetamide (δ 4.40, 3.55). In the case of *N*-benzyl-2-phenylacetamide, the –CH$_2$– signal at δ 3.55 ppm (s, 2H) was used to quantify the yield, based on the remaining phenylacetic acid reagent characterized by the signal at δ 3.48 ppm (s, 2H).

Results and discussion

Characterization of the ultra-small Zr-MOF nanoparticles

With the aim of studying the effect of linker modification on the catalytic performance of the Zr MOFs, we have prepared ultra-nanosized isoreticular UiO-topology MOFs with different linkers, summarised in Fig. 1, by adapting our coordination modulation protocols that used dichloroacetic acid as the modulator under excess linker conditions,[29] using acetic acid as the modulator instead (see section S. 2 of the ESI†). The powder X-ray diffraction (PXRD) patterns of the MOFs are rep-

resented in Fig. 2a and Fig. S1–S4,† confirming the UiO-type structural fingerprint through comparison to simulated patterns. Moreover, the broad XRD peaks are indicative of the small size of the nanoparticles, between 13 ± 4 and 40 ± 6 nm (see Table S1†), as determined by SEM analysis (Fig. S5–S13†). The broadening is more pronounced for the Zr-BDC-X (X = H, NH$_2$, NO$_2$, OH) materials with respect to the sharper peaks of the Zr-BPDC and Zr-NDC. This could be attributed to the slightly lower acidity of the extended linkers (predicted pK_{a1} BDC 3.51, NDC 3.69 and BPDC 3.77) slowing down self-assembly kinetics. Dynamic Light Scattering measurements of dispersions of the MOFs in methanol show minor aggregation of the samples – apart from Zr-NDC with no apparent aggregation – with hydrodynamic diameter varying from *ca.* 50 nm to *ca.* 250 nm (Fig. S14–S20†).

N_2 physisorption measurements of the samples, represented in Fig. 2b show that these small nanoparticles exhibit mesoporosity, together with a decrease in microporosity (see
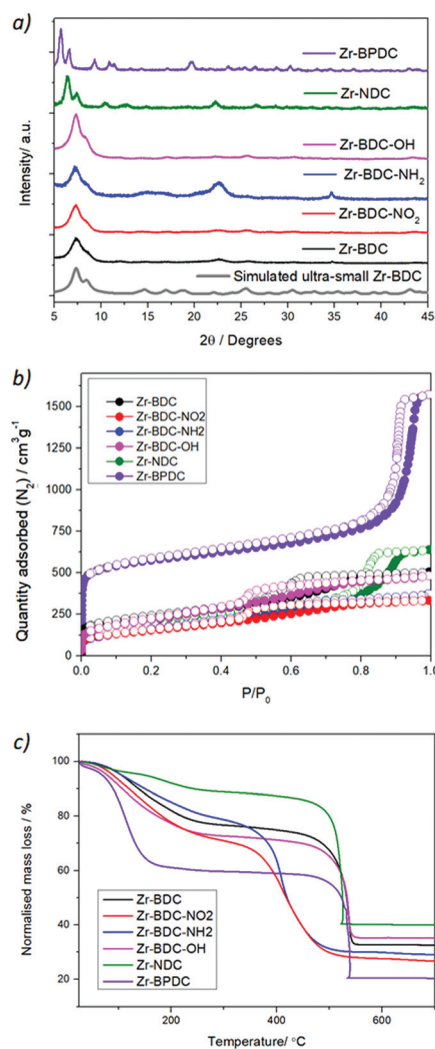
Fig. 2 Characterization of the Zr-MOFs by (a) PXRD together with simulated UiO-66 pattern with FWH 0.7, (b) N$_2$ adsorption and desorption isotherms and (c) TGA.

Fig. S21–S30†). This is in great agreement with reports showing that drastically reducing the particle size results in an increase in the mesoporosity and a decrease in the microporosity.[30] In particular, the Zr-BPDC sample exhibits the highest porosity (with a surface area of 2006 $m^2 g^{-1}$), while the Zr-BDC-OH, Zr-BDC-NO$_2$ and Zr-BDC-NH$_2$ are the less porous ones (452, 484 and 593 $m^2 g^{-1}$, respectively). However, the nanoparticles exhibit remarkably high pore volumes coming both from the induced mesoporosity (below P/P_0 = 0.9) and interparticle adsorption (above P/P_0 = 0.9), with twice the reported pore volume of pristine samples.[11,23,30]

Fourier transform infrared (FTIR) spectra of the samples were performed in order to confirm the presence of the functional groups in the benzene ring of the linker (*i.e.* NH$_2$, NO$_2$, OH), as indicated in Fig. S31 and S32.† The FTIR spectrum of the Zr-NDC sample indicates the absence of physisorbed water, suggesting high hydrophobicity, when compared with the rest of the samples. Additional information on the composition and defectivity (experimental linker-to metal ratio) of ultra-small nanoparticles can be extracted from the ^{1}H-NMR spectra of digested samples (see Table S3†) and thermogravimetric analysis of the MOFs (see Tables S4 and S5, and Fig. S33 and S34†). The molar ratio of modulator per linker (*i.e.* acetic and formic acid) oscillates between 0.14–1.1 for acetic acid, and 0.08–0.75 in the case of formic acid, despite the latter originating from the decomposition of DMF during synthesis, and the former being added to synthesis (*ca.* 18 equivalents) possibly due to the higher acidity of formic acid. The presence of formate defects in the catalysts is particularly relevant to aniline formylation, given formic acid is a reagent in this process. Although TGA cannot differentiate between the type of defect (*i.e.* missing linkers or missing clusters), it provides information about the linker to metal ratio.[31] The linker to metal ratio (L/Z$_r$ = 1 for the pristine materials) varied between 0.77 and 0.98, which corresponds to a molar percent of linker deficiency of 1.1% (for Zr-BDC-NO$_2$) and 22.9% (for Zr-NDC).[31] We have summarized the above-mentioned information about the samples' textural properties and linker/modulator incorporation – also described in the ESI† – in Table 1.

Catalytic activity of the ultra-small Zr-MOF nanoparticles

Once the materials were synthesized and characterized, they were applied as heterogeneous catalysts in amidation reactions, where the product formation was followed by liquid ^{1}H-NMR spectroscopic analysis of the reaction media (see Fig. S35–S55†). On the one hand, we started with aniline and formic acid as substrates for the direct amide bond formation of the formanilide product (see Scheme 1a). In the absence of a solvent, equimolar amounts of aniline and formic acid form a solid immediately on contact. This makes the isolation of the solid from the MOF difficult without the use of solvents, and so requires an excess of formic acid (*ca.* 5 eq.) for a neat, solvent-free reaction. The catalytic activity of the Zr-BDC-NH$_2$ sample over the blank autocatalytic reaction is shown in Table S6† and Fig. S35 and S36,† indicating higher reaction yields in the presence of the MOF for all reaction times sampled. In order to analyse the differences in the catalytic activity of the samples, solvent-free conditions and low conversion values at initial reaction times were employed to obtain the initial reaction rates, which allow assessment of catalytic activities and possible deactivation processes when the reactant concentration is far from depleted (see Table S7† and Fig. S38–S41†). The only samples that show catalytic activity in the formylation of aniline over the blank reaction (in the absence of MOF) were the NH$_2$ and NO$_2$-functionalized MOFs (see bars 2 and 3 in Fig. 3a).

Although exhibiting a moderate activity, both samples were slightly more active (initial reaction rate r_0 = 3.0 mmol h^{-1})
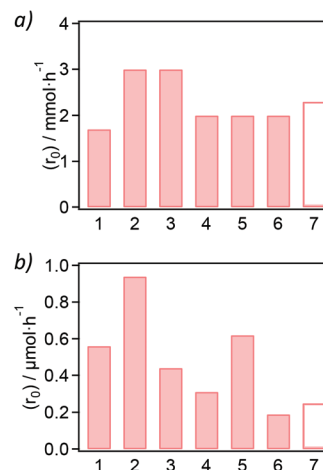

Fig. 3 Initial reaction rate for the formylation of aniline (a) and reaction between phenylacetic acid and phenylamine (b) using Zr-BDC (1), Zr-BDC-NO$_2$ (2), Zr-BDC-NH$_2$ (3), Zr-BDC-OH (4), Zr-NDC (5), Zr-BPDC (6) and blank reaction (7).

Table 1 Physicochemical properties of the Zr-MOF samples characterized (see ESI for more details†)

Zr-MOF	S_{area}/m^2 g^{-1}	Pore volume/cm^3 g^{-1}	NP size/nm	%HCOOH[a]	L/Zr	%ML[b]
Zr-BDC	894	0.74	13 ± 4	0.08	0.973	2.7
Zr-BDC-OH	452	0.49	15 ± 3	0.75	0.810	19.0
Zr-BDC-NO$_2$	484	0.53	28 ± 4	0.54	0.989	1.1
Zr-BDC-NH$_2$	593	0.69	18 ± 2	0.32	0.781	21.9
Zr-NDC	769	0.94	39 ± 6	0.15	0.771	22.9
Zr-BPDC	2006	2.33	39 ± 7	0.40	0.984	1.6

[a] Formic acid incorporated in the MOF from solvent breakdown. [b] Molar percent of linker deficiency (1-L/Zr × 100)

with respect to the blank reaction (r_0 = 2.3 mmol h^{-1}). The initial rate of aniline formylation in the presence of the non-functionalized Zr-BDC, Zr-BPDC and Zr-NDC is similar to the blank reaction (see bars 1 and 4–7 in Fig. 3a). The yields obtained (Table S7†) are in line with those reported in the literature in the case of UiO-66 (<5% yield) under similar reaction conditions.[27]

We have performed reusability of one of the best performing MOFs (Zr-BDC-NH$_2$) for 3 consecutive cycles, each of them with a reaction time of 30 minutes (see Fig. S42 and Table S8†). A minor decrease in product yield is observed (from 72% to 65%) likely due to the loss of part of the MOF powder during the centrifugation/re-dispersion cycles of the reusability testing. Both the presence of only traces of Zr (<0.51 wt% of the fresh MOF, assessed by ICP measurements) and the absence of ligand in the ^{1}H-NMR spectra suggest minimum leaching of metal and linker from the MOF to the reaction medium after the three catalytic cycles. The homogeneous Zr(IV) loading corresponding to this amount of leaching (<0.1 wt% with respect to aniline) has a negligible catalytic effect according to a previous report where 2–10 mol% ZrCl$_4$ is required as the catalyst of direct amidation of carboxylic acids with amines.[6] To assess the stability of the ultra-small Zr-MOF nanoparticles under these reaction conditions, we have measured their PXRD patterns after the reaction and compared them with those of the "as-prepared" samples (see Fig. S43–S48†). In general, the diffractograms show no major changes in the peaks' positions and width, which is indicative of the maintenance of their crystalline structure and particle size, apart from a minor crystallinity decrease for Zr-BPDC and Zr-NDC (see Fig. S47 and S48†). To further confirm the importance of the ultra-small nanoparticle size on the catalytic activity we have compared the activity of Zr-BDC-NH$_2$ with that of standard Zr-BDC-NH$_2$ (see Fig. S49 and S50† and Table S9†). While the nanosized (*ca.* 20 nm) MOF surpasses the activity of the blank reaction (34% yield), the standard Zr-BDC-NH$_2$ MOF (*ca.* 440 nm) gives a similar conversion to the blank autocatalytic reaction (22% yield) after 1 h.

On the other hand, we attempted the synthesis of *N*-benzyl-2-phenylacetamide by reacting phenylacetic acid and benzylamine in the presence of the Zr-MOF samples (5 mol%). As for the aniline formylation, the ^{1}H-NMR spectra of the reactions, calculated yields and rates are presented in Fig. S51† and Table S10,† respectively. Compared to the blank reaction, all Zr-MOF samples catalyze the amidation reaction between phenylacetic acid and benzylamine in deuterated methanol at 60 °C for 24 h, resulting in yields similar to what was recently published for UiO-66 (*ca.* 15% yield for *ca.* 5 mol% MOF loading). Fig. 3b shows that hydrophobic MOF materials such as the Zr-BDC-NO$_2$ (r_0 = 0.94 µmol h^{-1}) or Zr-NDC (r_0 = 0.62 µmol h^{-1}) present a higher activity than parent Zr-BDC (0.56 µmol h^{-1}) or the blank reaction (r_0 = 0.25 µmol h^{-1}). The yields of *N*-benzyl-2-phenylacetamide using Zr-BDC-NO$_2$ (see Table S10†) are comparable to the reported values for UiO-66 (10% mol) in ethanol as solvent at 80 °C (*ca.* 15%). However, the conditions reported here are milder in terms of temperature (60 °C) and MOF loading (5 mol%), which is half of the loading reported.[28] A higher yield can be obtained when the reaction time is increased to 72 h, obtaining a *ca.* 37% yield with the Zr-NDC catalyst, while no product is detected in the absence of a catalyst (see Fig. S52†). In addition, the catalyst shows good reusability with a minor decrease in catalytic activity that arises from loss of the powder during centrifugation/redispersion cycles, whereas the uncatalyzed reaction shows no conversion at any point (see Fig S53† and Table S11†).

Structure/composition-activity relationships of the ultra-small Zr-MOF nanoparticles

In the first place, we discuss the impact of the measured physicochemical properties (porosity, nanoparticle size and modulator/linker composition) of the ultra-small MOF nanoparticles on the calculated initial reaction rate of the two amidation reactions studied. We have represented the initial rate (r_0) for the reaction between aniline and formic acid (reaction A, abbreviated as $(r_0)_A$ in Fig. 4), as well as the reaction between phenylacetic acid and benzylamine, reaction B (abbreviated as $(r_0)_B$ in Fig. 4) for the different physicochemical properties (surface area, nanoparticle size, amount of formic acid modulator and amount of missing linkers) of the six Zr-MOF samples studied.

On the one hand, the surface area (and the related pore volume and % mesoporosity) of the samples does not have a clear influence on the rate of aniline formylation (see blue circles in Fig. 4a). In fact, the formylation rate is lower in the presence of the large surface area materials Zr-NDC and Zr-BPDC, compared with the higher rate achieved with low surface area materials Zr-BDC-NO$_2$ or Zr-BDC-NH$_2$. This suggests that the reaction between aniline and formic acid – substrates with small molecular sizes – is not controlled by diffusion and that the formylation is the rate-determining step. In contrast, a linear trend between these two variables (reaction rate and surface area) can be observed in the reaction between bulkier phenylacetic acid and benzylamine (see red squares in Fig. 4a), in the presence of Zr-BDC-OH (452 m^2 g^{-1}), Zr-BDC-NH$_2$ (593 m^2 g^{-1}), Zr-BDC (894 m^2 g^{-1}) and Zr-NDC (769 m^2 g^{-1}). The unexpected high and low reaction rates obtained with Zr-BDC-NO$_2$ (484 m^2 g^{-1}) and Zr-BPDC (2006 m^2 g^{-1}), respectively, may be a consequence of two facts: (i) the stronger Lewis acidity of Zr-BDC-NO$_2$ (with electron-withdrawing -NO$_2$ groups); or (ii) the lower stability of Zr-BPDC (due to rotation of the biphenyl group), which is further suggested by the poorer crystallinity, as assessed by PXRD, of the spent material. In the case of Zr-BDC-OH and Zr-BDC-NH$_2$, the presence of electron-donating groups and thus weaker Lewis acidity of the Zr sites might also decrease their catalytic activity in addition to the surface area effect.

On the other hand, the size of the ultra-small Zr-MOF nanoparticles presents an optimal value of *ca.* 20–25 nm to increase the reaction rate of amide bond formation in the two examples studied here (see Fig. 4b). This is especially clear in the case of aniline formylation, where Zr-BDC-NO$_2$ (*ca.* 28 nm) and Zr-

● Reaction A (aniline formilation)   ■ Reaction B (phenylacetic acid and phenylamine)
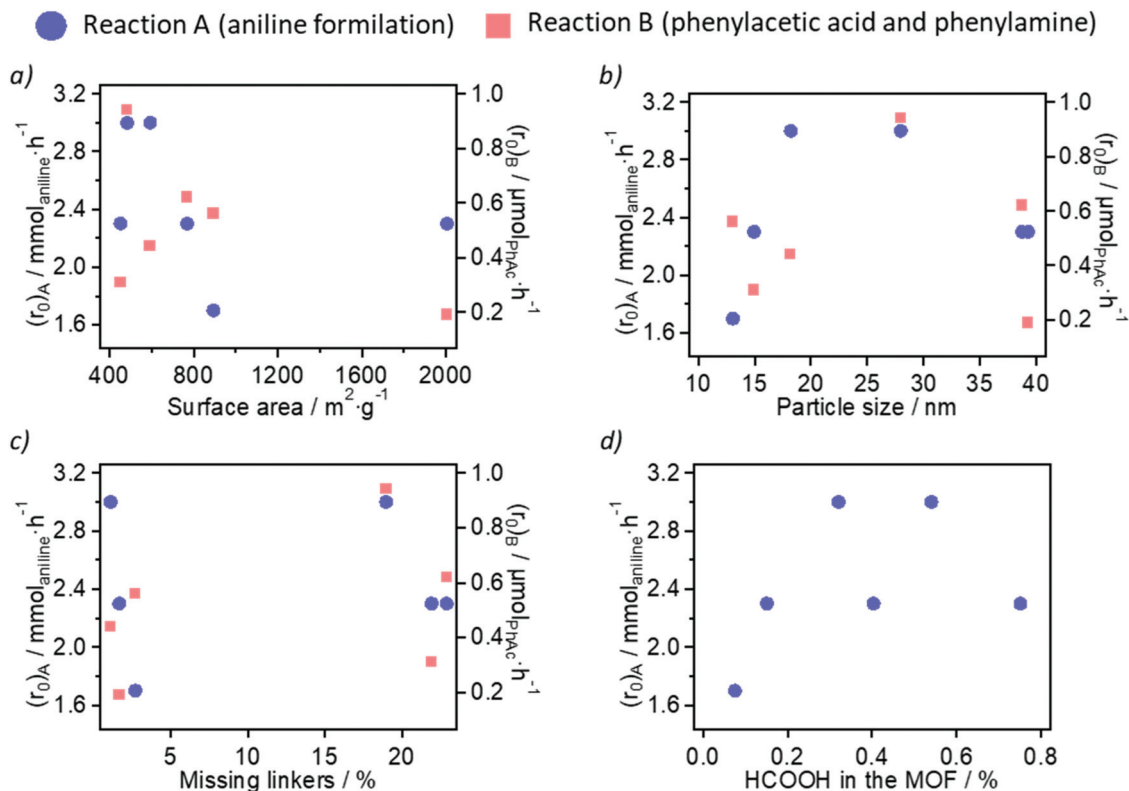
Fig. 4 Initial reaction rate for the formylation of aniline (blue circles) and reaction between phenylacetic acid and phenylamine (red squares) with respect to: (a) surface area; (b) nanoparticle size; (c) missing linkers and (d) HCOOH present in the MOF as FA per L molar ratio (only for the formylation reaction).

BDC-NH₂ (*ca.* 18 nm) are the most active catalysts. Lower (Zr-BDC and Zr-BDC-OH) and higher (Zr-NDC and Zr-BPDC) nanoparticle sizes are related to lower reaction rates. Despite the lower sizes of Zr-BDC and Zr-BDC-OH nanoparticles (13 and 15 nm, respectively) increasing the availability of catalytic Zr_6 sites on particle external surfaces, the larger Zr-BDC-NO₂ nanoparticles increase the rate of both reactions to a higher extent. As proposed in the discussion of the surface area (as well as in literature),[22,23] the stronger acidity and hydrophobicity of Zr-BDC-NO₂ may be the keys to its differential behaviour.

Regarding the sample composition and potential defectivity, two variables were studied: the molar percent of linker deficiency (obtained from TGA) and the incorporation of formate ions (obtained from ¹H-NMR spectroscopy) in the MOFs, which although came from the decomposition of DMF during synthesis are more significantly incorporated than the added acetate ions in some cases. The molar percent of linker deficiency in Zr-BDC, Zr-BDC-NO₂ and Zr-BPDC is significantly lower (1–3%) than in Zr-BDC-OH, Zr-BDC-NH₂ and Zr-NDC (19–23%). However, no clear dependence of the reaction rate on the missing linker density can be established at this point (see Fig. 4c). The relationship between the formylation rate and the %HCOOH is plotted in Fig. 4d, suggesting that moderate concentrations of HCOOH in the MOF (*ca.* 0.5 FA per linker) are beneficial for their catalytic activity in the formylation of aniline; adsorbed formate intermediates have been pro-

posed for other solid acid catalysts of amide bond formations.[32] However, larger amounts of this modulator are detrimental for the MOF catalytic activity, probably due to extensive coordination to the CUSs at the Zr-oxo clusters, thus decreasing the number of active sites.[22] It should be noted that the additional formate introduced into the reactions by the catalyst is minimal when comparing the 5 mol% catalyst loading to the 5-fold excess of formic acid used.

Performance of the ultra-small Zr-MOF nanoparticles with respect to benchmark heterogeneous catalysts

To put the reaction rates obtained with the ultra-small MOF nanoparticles in context, in this section we will compare them with benchmark solid catalysts reported in the literature (see Table 2). In the case of the formylation of aniline, the activity of parent Zr-BDC using methanol as solvent at 35 °C was recently reported by Timofeeva *et al.*[27] Poor formanilide yields, <1% after 90 min, were obtained, which were associated with a low reaction rate <0.67 mmol h⁻¹ g_{MOF}^{-1}, whereas we have tested the ultra-small Zr-BDC-NH₂ MOF under the same conditions (deuterated methanol as the solvent), which showed a decrease in catalytic activity in comparison with solvent-free conditions (See Fig. S55† and Table S12†), but outperforming the reported UiO-66.[27] In contrast, both functionalized ultra-small Zr-BDC-NH₂ and Zr-BDC-NO₂ nanoparticles enhance the solvent-free formylation of aniline with a reaction rate of

**Table 2** Catalytic performance of Zr-MOF samples with respect to benchmark heterogeneous catalysts

Catalyst	Temperature/°C	Solvent	HCOOH: aniline	Yield (reaction time)	Activity/mmol h^{-1} $g_{catalyst}^{-1}$	Ref.
Zr-BDC-NH$_2$	35	Solvent-free	5	72% (0.5 h)	300	This work
MOF-808	35	Solvent-free	2	95% (0.3 h)	864	27
UiO-66	35	Methanol	1.2	<1 (1.5 h)	<1	27
ZnO	25	Solvent-free	4	70% (0.16 h)	4.5	33
Al$_2$O$_3$	40	Solvent-free	3	98% (0.08 h)	2147	34

300 mmol h^{-1} g_{MOF}^{-1} (obtained from the initial reaction rate value of 3 mmol h^{-1} calculated in Table S6† and the 0.01 g of MOF catalyst employed). This value is of the same order of magnitude as that reported for benchmark material MOF-808 (864 mmol h^{-1} g_{MOF}^{-1}) under solvent-free conditions at 35 °C.[27] The activity of the Zr-MOFs for the formylation of aniline is higher than other metal oxides reported as heterogeneous catalysts of this reaction, such as ZnO at 25 °C (4.5 mmol h^{-1} g_{ZnO}^{-1}) or even at 70 °C (69 mmol h^{-1} g_{ZnO}^{-1}).[33] However, the studied Zr-MOFs are clearly outperformed by nanocrystalline Al$_2$O$_3$ (*ca.* 40 nm), which promotes the neat *N*-formylation of aniline at 40 °C, with a reaction rate of 2147 mmol h^{-1} g Al$_2$O$_3^{-1}$.[34]

For the synthesis of *N*-benzyl-2-phenylacetamide from the reaction between phenylacetic acid and benzylamine, Francisco de Azambuja *et al.* obtained a 14% yield of amide product after 24 h in the presence of UiO-66 (10 mol%) in ethanol at 80 °C.[28] This is associated with a reaction rate of *ca.* 35 μmol h^{-1} g_{MOF}^{-1}, a smaller value than the 94 μmol h^{-1} g_{MOF}^{-1} obtained with Zr-BDC-NO$_2$ under milder conditions (methanol-d at 60 °C) with 5 mol% of catalyst.

Mechanism for the direct amide bond formation at ultra-small Zr-MOF nanoparticles

For both amide bond formations studied here, the higher reaction rate (or similar rate but at a lower temperature) obtained with the ultra-small nanoparticles with respect to standard UiO-66 reported[27,28] highlights the facilitation of mass transport in the ultra-small nanoparticles. In the reaction of bulky substrates, such as benzylamine and phenylacetic acid, the key role of surface area on the activity was discussed in Fig. 4a. These results indicate the participation of Zr open sites in the functionalized Zr-BDC-NO$_2$/NH$_2$ materials acting as Lewis acids. During this study, the use of polar solvents such as DMSO lowers the activity of the Zr-BDC to the levels of the blank reaction, probably due to solvent coordination and poisoning of those sites. Azambuja *et al.* proposed a computational-based reaction mechanism (using alcohols as solvents) highlighting the Lewis acid activation of carboxylate groups of the carboxylic acid substrate by Zr sites, and proton transfer to the alkoxy ligand, resulting from the solvent coordination to the Zr open metal sites on adjacent Zr$_6$ SBUs.[28] The uptake of HCOOH modulator as charge-compensating defects in catalytically active Zr-BDC-NO$_2$/NH$_2$ samples (Fig. 4d) points to this type of dissociative carboxylic acid coordination to the Zr-oxo cluster, already reported in metal oxide amidation catalysts.[32,35]
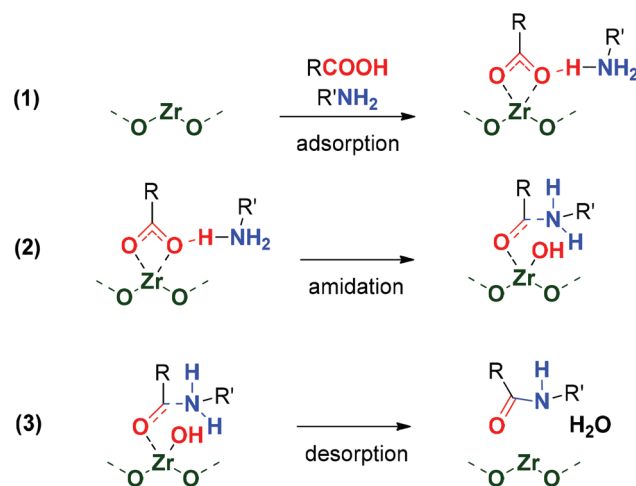
Scheme 2 Proposed mechanism of amide bond formation with Zr-MOFs.

Therefore, we propose the dissociative adsorption of the carboxylic acid at the Zr-oxo cluster due to the high oxophilicity of these SBUs, as a previous step to the nucleophilic attack of the amine and water elimination (see Scheme 2). In this sense, little information has been offered on the process of water elimination (to form the amide bond) during the reaction mechanism from the point of view of the materials' properties, such as the hydrophobicity of the material. We propose that the hydrophobicity of the MOF increases its catalytic activity. This is indicated by the low water content of the Zr-NDC sample, evident in its FTIR spectrum (Fig. S31†), which contains a naphthalene moiety with respect to benzene or biphenyl-based MOFs, resulting in high catalytic activity in the synthesis of *N*-benzyl-2-phenylacetamide. In contrast, more hydrophilic H-bond forming OH and NH$_2$-functionalized linkers in Zr-BDC-OH and Zr-BDC-NH$_2$ might be detrimental to the water desorption step, in line with their poor activity in the synthesis of *N*-benzyl-2-phenylacetamide. Besides the hydrophobicity, the high activity of Zr-BDC-NO$_2$ might also be related to its stronger Lewis acidity and hydrophobicity based on our previous results.[22,23,36]

Conclusions

The application of Zr-MOF nanoparticles as heterogeneous catalysts for the synthesis of amide bonds from carboxylic acids

and amines is an emerging area of research in the application of MOF-based catalysts to organic synthesis, due to the industrial and biological importance of amides. Although Zr-based CUSs are traditionally reported as presenting Lewis acid active sites, to establish a correlation between the physicochemical properties of Zr-MOFs and their catalytic activity is a challenging and complex task. Herein we have unravelled key properties that influence the amidation reaction rate, such as surface area, defectivity, modulator incorporation, and the presence of hydrophobic or electron-withdrawing linkers. The ultra-small Zr-MOF nanoparticles outperform some of the heterogeneous catalysts reported in the literature, including other MOFs and metal oxides. With this MOF characterization and kinetic studies, we expect to contribute to the re-design of the MOF structure and composition in order to boost its catalytic activity for the transformation carboxylic acids and amines into relevant amides.

Author contributions

All authors contributed to conceptualization, methodology, analysis, investigation, writing—original draft preparation and editing. All authors have read and agreed to the published version of the manuscript.

Conflicts of interest

There are no conflicts to declare

Acknowledgements

Notes and references

1 N. Martin and F. G. Cirujano, *Catal. Commun.*, 2022, **164**, 106420.
2 V. R. Pattabiraman and J. W. Bode, *Nature*, 2011, **480**, 471.
3 S. D. Roughley and A. M. Jordan, *J. Med. Chem.*, 2011, **54**, 3451.
4 J. R. Dunetz, J. Magano and G. A. Weisenburger, *Org. Process Res. Dev.*, 2016, **20**, 140.
5 H. Lundberg, F. Tinnis, N. Selander and H. Adolfsson, *Chem. Soc. Rev.*, 2014, **43**, 2714.
6 H. Lundberg, F. Tinnis, J. Zhang, A. G. Algarra, F. Himo and H. Adolfsson, *J. Am. Chem. Soc.*, 2017, **139**, 2286.
7 J. Cossy and C. Palegrosdemange, *Tetrahedron Lett.*, 1989, **30**, 2771.
8 A.-X. Li, T.-S. Li and T.-H. Ding, *Chem. Commun.*, 1997, 1389.
9 N. Narender, P. Srinivasu, S. J. Kulkarni and K. V. Raghavan, *Green Chem.*, 2000, **2**, 104.
10 K. Komura, Y. Nakano and M. Koketsu, *Green Chem.*, 2011, **13**, 828.
11 L. Valenzano, B. Civalleri, S. Chavan, S. Bordiga, M. H. Nilsen, S. Jakobsen, K. P. Lillerud and C. Lamberti, *Chem. Mater.*, 2011, **23**, 1700.
12 P. Valvekens, F. Vermoortelea and D. De Vos, *Catal. Sci. Technol.*, 2013, **3**, 1435.
13 V. Pascanu, G. González-Miera, A. K. Inge and B. Martín-Matute, *J. Am. Chem. Soc.*, 2019, **141**, 7223.
14 A. Bavykina, N. Kolobov, S. Khan, J. A. Bau, A. Ramirez and J. Gascon, *Chem. Rev.*, 2020, **120**, 8468.
15 Y.-S. Wei, M. Zhang, R. Zou and Q. Xu, *Chem. Rev.*, 2020, **120**, 12089.
16 X. Feng, H. Sekhar-Jena, C. Krishnaraj, K. Leus, G. Wang, H. Chen, C. Jia and P. Van Der Voort, *ACS Appl. Mater. Interfaces*, 2021, **13**, 60715.
17 N. Martín and F. G. Cirujano, *Org. Biomol. Chem.*, 2020, **18**, 8058.
18 F. G. Cirujano, R. Luque and A. Dhakshinamoorthy, *Molecules*, 2021, **26**, 1445.
19 F. G. Cirujano and A. Dhakshinamoorthy, *Adv. Sustainable Syst.*, 2021, **5**, 2100101.
20 F. G. Cirujano and A. Dhakshinamoorthy, *ChemCatChem*, 2021, **13**, 4679.
21 F. G. Cirujano and A. Dhakshinamoorthy, *New J. Chem.*, 2022, **46**, 1469.
22 F. G. Cirujano and F. X. Llabrés i Xamena, *J. Phys. Chem. Lett.*, 2020, **11**, 4879.
23 G. Fu, F. G. Cirujano, A. Krajnc, G. Mali, M. Henrion, S. Smolders and D. E. De Vos, *Catal. Sci. Technol.*, 2020, **10**, 4002.
24 I. Abánades Lázaro, C. Popescu and F. G. Cirujano, *Dalton Trans.*, 2021, **50**, 11291.
25 J. M. Guarinos, F. G. Cirujano, A. Rapeyko and F. X. Llabres i Xamena, *Mol. Catal.*, 2021, **515**, 111925.
26 L. T. M. Hoang, L. H. Ngo, H. L. Nguyen, H. T. H. Nguyen, C. K. Nguyen, B. T. Nguyen, Q. T. Ton, H. K. D. Nguyen, K. E. Cordova and T. Truong, *Chem. Commun.*, 2015, **51**, 17132.
27 M. N. Timofeeva, V. N. Panchenko, I. A. Lukoyanov and S. H. Jhung, *React. Kinet., Mech. Catal.*, 2021, **133**, 355.
28 F. de Azambuja, A. Loosen, D. Conic, M. van den Besselaar, J. N. Harvey and T. N. Parac-Vogt, *ACS Catal.*, 2021, **11**, 7647.
29 I. Abánades Lázaro, S. Abánades Lázaro and R. S. Forgan, *Chem. Commun.*, 2018, **54**, 2792.
30 M. Taddei, K. Corinna-Dümbgen, J. A. van Bokhoven and M. Ranocchiari, *Chem. Commun.*, 2016, **52**, 6411.
31 I. Abánades Lázaro, *Eur. J. Inorg. Chem.*, 2020, **2020**, 4284.
32 F. Arena, C. Deiana, A. F. Lombardo, P. Ivanchenko, Y. Sakhno, G. Trunfio and G. Martra, *Catal. Sci. Technol.*, 2015, **5**, 1911.
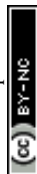
33 M. Hosseini-Sarvari and H. Sharghi, *J. Org. Chem.*, 2006, **71**, 6652.

34 V. Kumar, D. Rashmi, R. Devi, P. Kumar-Raul and A. Jyoti-Thakur, *Green Chem.*, 2012, **14**, 847.

35 C. Deiana, Y. Sakhno, M. Fabbiani, M. Pazzi, M. Vincenti and G. Martra, *ChemCatChem*, 2013, **5**, 2832.

36 I. Abánades Lázaro, *J. Mat. Chem. A.*, 2022, DOI: **10.1039/D2TA00603K**, just accepted.